

Microstructural Analysis of Linear Friction-Welded 718 Plus Superalloy

K.R. VISHWAKARMA,^{1,3} O.A. OJO,¹ P. WANJARA,²
and M.C. CHATURVEDI¹

1.—Department of Mechanical and Manufacturing Engineering, University of Manitoba, Winnipeg, MB R3T 5V6, Canada. 2.—National Research Council Canada, Montreal, PQ H3T 2B2, Canada. 3.—e-mail: krutika.vishwakarma@umanitoba.ca

The microstructure of Allvac 718 Plus (718 Plus; ATI, Pittsburgh, PA, USA) superalloy was examined after linear friction welding (LFW) and after standard postweld heat treatment (PWHT). The liquid phase reaction of second-phase precipitates, which are known to constitutionally liquate during conventional fusion welding, was observed in the thermomechanically affected zone (TMAZ) of the welded material. These phases included MC-type carbides, Ti-rich carbonitrides, and δ phase precipitates. This observation is contrary to the general assumption that LFW is a completely solid-state joining process. However, unlike conventional fusion welding processes that cause heat-affected zone liquation cracking in 718 Plus and many other superalloys, the LFW process did not cause cracking in 718 Plus superalloy despite the liquation of precipitates. This absence of cracking during joining is attributed to the applied compressive stress during the forging stage of the LFW process. Also, no cracking was observed after PWHT, although PWHT resulted in a microstructure that had a nonhomogeneous distribution of precipitates in the weld and the TMAZ.

INTRODUCTION

Allvac 718 Plus (718 Plus; ATI, Pittsburgh, PA) was developed from conventional Inconel 718 to have a higher working temperature and superior creep properties while maintaining good formability. It can be used at temperatures up to 700°C, which is about 50°C higher than the upper temperature limit for Inconel 718, and it has creep strength similar to that reported by Waspaloy (United Technologies Corp., Hartford, CT).¹ 718 Plus is precipitation strengthened by the ordered γ' phase, although it has a lower volume fraction compared to other γ' -strengthened alloys. Previous investigations on fusion welding of 718 Plus using electron beam (EB)² as well as laser beam³ showed that 718 Plus undergoes heat-affected zone (HAZ) microfissuring during welding and postweld heat treatment (PWHT) due to liquation effects.

Linear friction welding (LFW) offers an attractive alternative to the conventional welding processes used for manufacturing and repair of aerospace components. It involves joining of components using

frictional heat produced by their relative motion and the applied forging pressure. The LFW process can be broadly classified into four distinctive steps, as outlined by Varis et al.⁴: (I) the initial stage where sufficient heat is generated due to solid friction, (II) the transition stage where the contact moves beyond the interface expelling the asperities, (III) the equilibrium stage that involves further generation of heat and joining at the interface, and (IV) the deceleration stage where the movement of the components is stopped and followed by the application of a forging pressure. The resulting microstructure consists of the weld interface, the thermomechanically affected zone (TMAZ), and the unaffected base alloy. Depending on the position in the weldment, different regions of the TMAZ and the base alloy are subjected to different ranges of temperatures and plastic deformation that influence microstructural development. LFW has been successfully used to join steel⁵ and titanium alloys^{6,7} in applications including manufacturing and repair of turbine components. For Ni-base superalloys, LFW has been used to weld polycrystalline,⁸

cast,⁹ dissimilar,¹⁰ and single-crystal materials.¹¹ This joining process is generally considered to be a completely solid-state joining process,¹² and like other friction-welding processes, it could eliminate problems associated with melting and resolidification of conventional fusion welding techniques. However, some recent studies suggest that liquation does occur in TMAZ during the LFW process in single-crystal CMSX-486¹³ and IN 738,¹⁴ although no such study exists for 718 Plus alloys. As liquation could result in microfissuring, LFW was used to weld 718 Plus to examine the feasibility of the technique and its effect on the microstructure of the alloy. The results of the study are presented and discussed in this article.

EXPERIMENTAL PROCEDURES

The as-received 718 Plus alloy was in the form of 15.9 mm × 304.8 mm × 127 mm hot-rolled plates with a chemical composition of (wt.%) 17.92 Cr, 9.00 Co, 52.18 Ni, 9.33 Fe, 1.50 Al, 0.74 Ti, 5.51 Nb, 2.68 Mo, 1.04 W, 0.003 B (30 ppm), and 0.006 P (60 ppm). Test coupons measuring 12.8 mm × 11.1 mm × 17.7 mm were machined from the as-received plates and were solution treated at 950°C for 1 h followed by water quenching. Prior to welding, the contact surfaces of the coupons were ground and cleaned with alcohol. LFW was performed at ambient temperature under prevailing atmospheric conditions using an MTS LFW Process Development System (PDS; MTS, Eden Prairie, MN, USA) located at the National Research Council of Canada. The technical specifications of the equipment are described elsewhere.¹⁵ Previous work on LFW of Inconel 718 using processing conditions of 80 Hz for the frequency (f), 2 mm for the amplitude (a), 70 MPa for the forging pressure (P), and 2 mm for the axial shortening (s) indicated that only the center section of the welded coupons was bonded.¹⁶ To extend bonding to the periphery regions, in the current work on LFW of 718 Plus, the frequency was increased to 100 Hz and the pressure to 90 MPa. Welded specimens were subjected to the standard PWHT, which consisted of holding at 950°C for 1 h followed by air cooling, aging at 718°C for 2 h, and then at 650°C for 8 h followed by air cooling. Cross sections of the as-welded and postweld heat-treated samples in the long transverse direction were used for microstructural analysis. Metallographic specimens were etched by swabbing using modified Kalling's reagent and electrolytically in 10% oxalic acid. Samples were also electrolytically etched in a mixture of 12 mL H₃PO₄ + 40 mL HNO₃ + 48 mL H₂SO₄ at 6 V for 5–6 s to reveal the γ' phase in the microstructure. The weld zone, base alloy, and TMAZ microstructures were examined and analyzed using an optical microscope, JEOL 5900 scanning electron microscope (SEM; JEOL Ltd., Tokyo, Japan) equipped with an ultrathin window energy dispersive spectrometer (EDS; Oxford Instruments, Oxfordshire, UK), and JEOL 2000

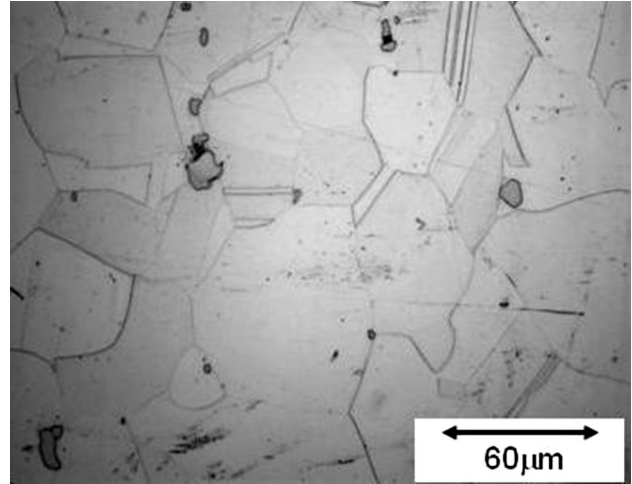


Fig. 1. Light optical image of the microstructure of as-received 718 Plus showing randomly distributed second-phase particles.

FX transmission electron microscope (TEM). Thin foils for TEM were produced by twin-jet polishing with 10% perchloric acid in 90% methyl alcohol at a temperature of -20°C to -30°C with a current of 1.5 A current and a voltage of 2 V. The grain size distribution across the weld joint was also examined by electron backscatter diffraction (EBSD)-based orientation imaging microscopy (OIM) equipped on Phillips XL 80 environmental scanning electron microscope (ESEM; Philips, Amsterdam, The Netherlands).

RESULTS AND DISCUSSION

As-received and Solutionized Microstructure

The as-received microstructure of 718 Plus consisted of a face-centered cubic (fcc) γ matrix with randomly dispersed second-phase particles as shown in the optical micrograph in Fig. 1. SEM/EDS analysis was used to identify the second-phase particles by their morphology and chemical composition. Blocky particles, shown in Fig. 2a, were predominantly rich in Nb with a small percentage of Ti and were identified to be MC-type carbides, whereas the irregular-shaped particles shown in Fig. 2b were mainly Ti-rich carbonitrides. The composition of these particles, as determined by the SEM/EDS semiquantitative analysis, is presented in Table I alongside the matrix composition. The other commonly found precipitate in 718 type alloys is the orthorhombic δ phase, which was not observed in the microstructure of 718 Plus alloy. The absence of δ phase in the as-received microstructure may be due to the use of a homogenization heat-treatment temperature that was above the solvus temperature of the δ phase followed by rapid cooling. Thin foils examined in TEM also revealed the presence of fine particles, as shown in Fig. 3. The inset in Fig. 3b shows that the selected-area diffraction pattern (SADP), obtained in [001] thin-foil

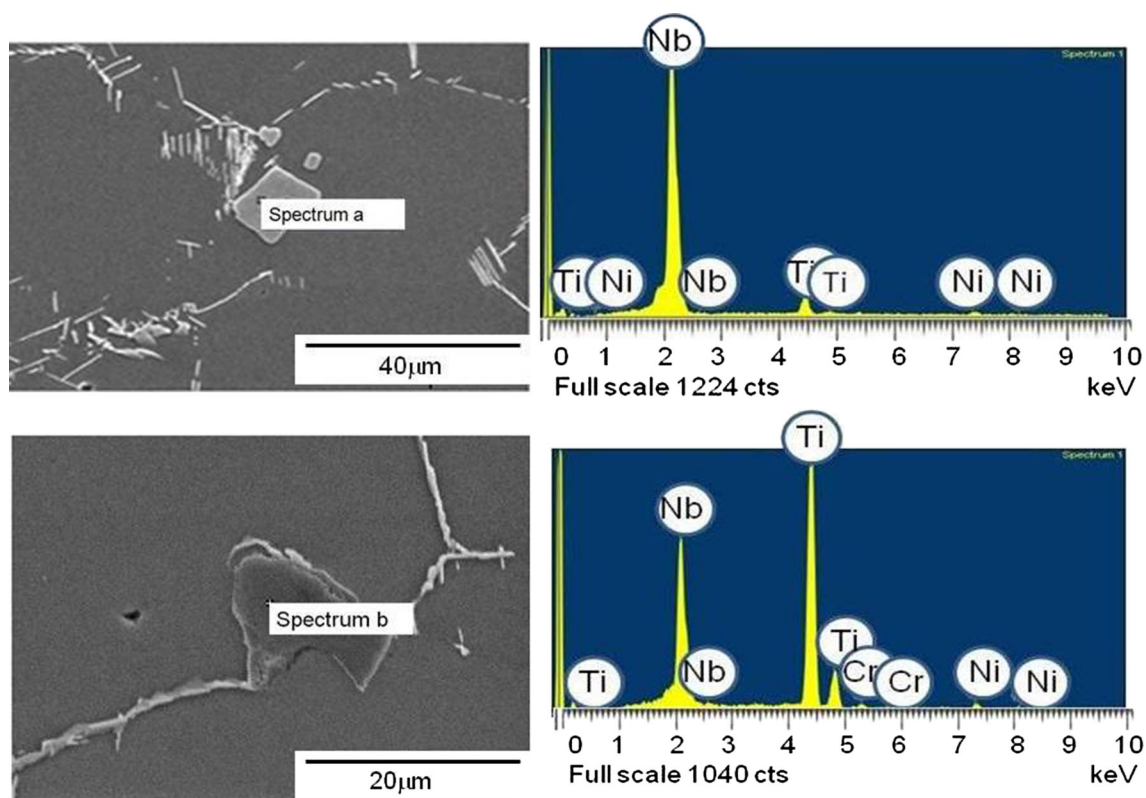


Fig. 2. (a) NbC particle with the EDS spectrum and (b) Ti(C,N) particle with the EDS spectrum.

Table I. Average chemical composition of the second-phase particles and matrix as determined by SEM EDS analysis in 718 Plus alloy

wt.%	Matrix	NbC	Ti(C,N)	Laves phase	δ phase
Al	1			1	2
Ti	1	8	63	5	1
Cr	18	1	5	16	17
Fe	9		2	8	9
Co	10			9	10
Ni	53	2	10	50	55
Nb	4	89	20	11	6
Mo	3				3
W	1			2	1

orientation, contained the (100)-type superlattice reflections in it, suggesting the precipitates to be γ' phase. The dark-field image taken from one such reflection confirms the identity of these particles to be γ' phase. Table II lists the average grain size of the as-received material and presents the approximate sizes of the phases as observed in the microstructure.

Figure 4 shows the microstructure of 718 Plus after solutionizing at 950°C for 1 h followed by water quenching. The amount and distribution of the MC-type carbides and Ti-rich carbonitrides was not considerably altered by the heat treatment (Fig. 5a), but the heat treatment resulted in the precipitation

of δ phase particles. The orthorhombic δ phase was mostly present at the grain boundaries, with either small or large needle-like morphology or in the platelet form. The major strengthening precipitates of the alloy γ' were uniformly distributed throughout the microstructure, as shown in Fig. 5b.

As-welded Microstructure

The LFW process produced integral crack-free welds in the 718 Plus alloy. Figure 6 shows a low-magnification optical micrograph of the microstructure of the as-welded 718 Plus alloy. The microstructure can be divided into three distinct zones, as identified in the micrograph, specifically, the base alloy matrix, TMAZ, and the weld center.

In comparison to the previous work on Inconel 718¹⁶ the current processing conditions of higher frequency and pressure produced an integral weld along the entire cross section of the joint. In the current work, except for a few carbides, the weld region did not comprise of any second-phase particles, such as δ phase and γ' precipitates. The most striking feature of the weld center was the change in the grain size. A comparison of the grain sizes in the base alloy and that in the weld center is shown in an optical micrograph in Fig. 7. This is further corroborated by EBSD-based orientation mapping (Fig. 8) showing individual grains in random colors for the weld center and the base alloy. The average grain size in the weld zone was observed to be significantly

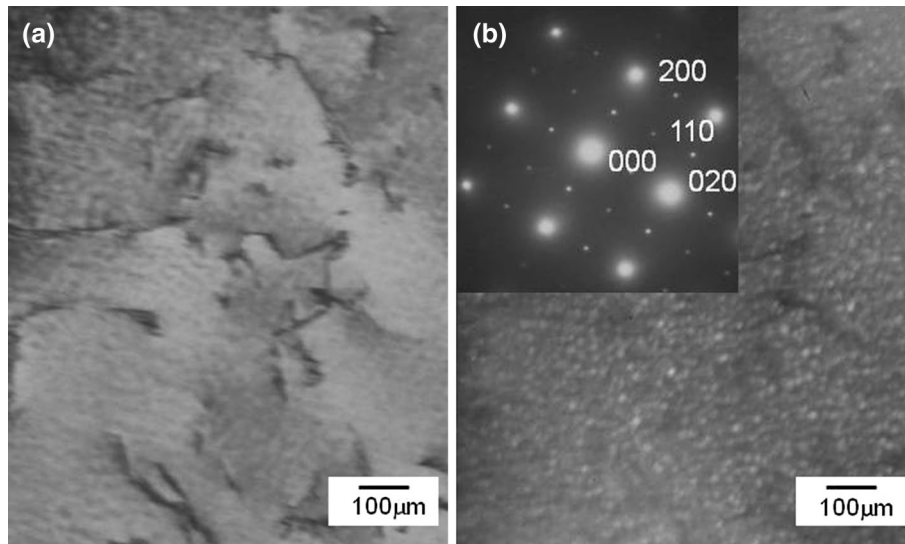


Fig. 3. As-received 718 Plus alloy: (a) bright-field image of the matrix and (b) selected-area diffraction pattern in the direction parallel to [001] zone axis.

smaller than it was in the base alloy. That is, across a region of about $30\ \mu\text{m}$ from the weld line, the grain size was about $3\ \mu\text{m}$ as compared to the $50\text{-}\mu\text{m}$ grain size of base alloy (Table II). Beyond $30\ \mu\text{m}$ from the weld line, the grain size increased progressively, inevitably due to recrystallization kinetics (i.e., decreasing Zener–Holloman parameter), which stems from the gradients in temperature and strain as reported recently for linear friction-welded Waspaloy.¹⁷ At about $100\ \mu\text{m}$ from the weld line, the average grain size in the TMAZ was similar to that of the base alloy. The fine recrystallized grains in the weld center were also observed by Ola et al.¹⁴ in the linear friction-welded Inconel 738. They suggested that the presence of such fine grains could not be solely explained by classic solid-state recrystallization theory and may be associated with the liquation and resolidification of phases within the alloy. The nonequilibrium liquation phenomenon and the strain-induced rapid solidification were proposed to explain the formation of fine grains in the weld center.^{14,18} The fine grain size is a characteristic feature of the linear friction welds, which has been also observed in Inconel 718¹⁵ and Waspaloy.¹⁹

Microstructural characterization of the TMAZ in the linear friction welds showed features that were consistent with grain boundary liquation and constitutional liquation of second-phase particles, as was observed during fusion welding of 718 Plus alloy.² Liquation is generally not expected during a solid-state joining process, like LFW, because the temperature reached during the process is below the solidus temperature of the alloy. However, subsolidus liquation can occur by nonequilibrium processes like constitutional liquation of second-phase particles and by lowering of the melting point of the alloy due to segregation of melting point depressants.

Constitutional liquation, as proposed by Pepe and Savage in 1967^{7,20} states that localized melting is possible below the equilibrium solidus temperature of the alloy when a rapid heating rate is involved. During LFW, the heating rate has been suggested to be as high as $368^\circ\text{C/s} \pm 140^\circ\text{C/s}$,¹⁹ which could induce nonequilibrium liquation of second-phase particles. Constitutional liquation of second-phase particles during conventional fusion welding processes has been observed in 718 Plus alloy; however, its occurrence in linear friction welds has not been reported previously.

In the current work, many grain boundaries were observed to have liquated, with the presence of characteristic resolidified phases on them, as shown in Fig. 9. The liquated grain boundaries in the TMAZ were distinctly of two types, as marked “A” in Fig. 10 and type B as shown in a higher magnification image of the TMAZ region (inset of Fig. 10). Type A grain boundaries were devoid of any precipitates, which is in contrast to the precipitate bearing type B grain boundaries. The grain boundaries of type A had a conspicuously different wavy pattern of resolidification. The zigzag nature of these grain boundaries is typical of liquid film migration (LFM). LFM has been observed in the HAZ of several Ni-base superalloys welded by conventional fusion welding techniques and linear friction-welded IN 738 superalloy.^{3,21,22} Under certain conditions, liquated regions of grain boundaries in the HAZ in these alloys can solidify via LFM instead of the normal solidification mode that result in the formation of resolidified products. LFM, on the other hand, is a faster solidification mode and can result in resolidified products being not present on them depending on the thickness of the liquated grain boundary and the concentration of alloying elements of the liquid.²¹

Table II. Average grain size in as-received, as-welded, and postweld heat-treated 718 Plus and approximate sizes of the various phases as observed in the microstructure

	As-welded			Postweld heat-treated			
	As-received	Base alloy	TMAZ	Weld center	Base alloy	TMAZ	Weld center
Grain size (μm)	47 ± 5	54 ± 6	Increases from weld center to base alloy	3 ± 2	54 ± 6	Increases from weld center to base alloy	< 10
Approximate sizes of the various phases NbC and Ti(C,N) γ' phase Laves phase δ phase	$(0.5-20 \mu\text{m})$ $< 20 \text{ nm}$ $< 0.5 \mu\text{m}$ thin needles	$(0.5-20 \mu\text{m})$ $< 20 \text{ nm}$ $< 0.5 \mu\text{m}$ thin needles	$1-10 \mu\text{m}$		$(0.5-20 \mu\text{m})$ $< 20 \text{ nm}$ $< 0.5 \mu\text{m}$ thin needles	$1-10 \mu\text{m}$ $< 0.5 \mu\text{m}$ thin needles	$< 0.5 \mu\text{m}$ thin needles

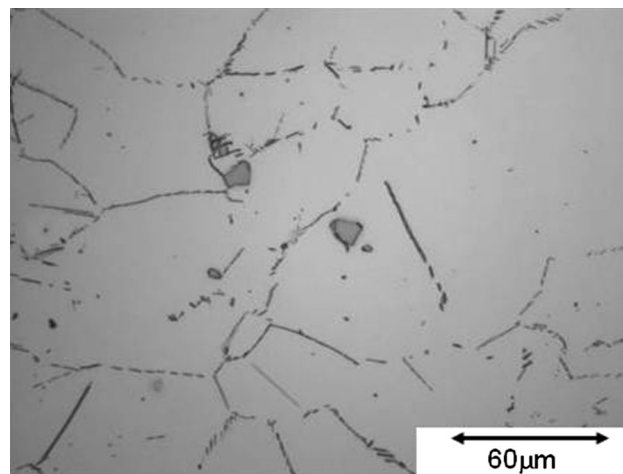


Fig. 4. Light optical image of the as-welded base alloy microstructure.

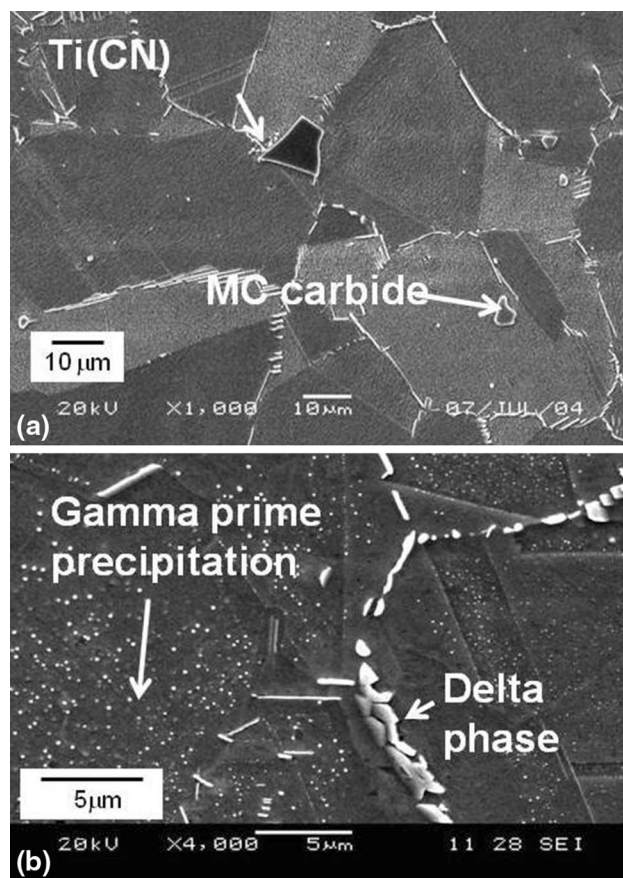


Fig. 5. (a) Secondary electron image of the as-welded base alloy showing gamma prime particles and delta phase at the grain boundaries (etched by gamma prime etchant) and (b) shows MC carbides and carbonitride particles (etched by Kalling's etchant).

Grain boundaries such as type B, shown in inset of Fig. 10 were carefully analyzed using SEM EDS analysis to study the nature of the phases present, and Table I shows the chemical composition of one

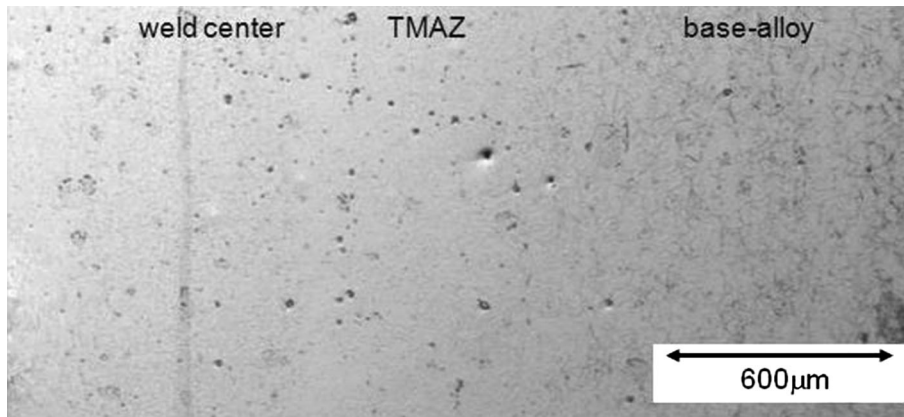


Fig. 6. Microstructure of the linear friction-welded 718 Plus showing the weld center, TMAZ, and the base alloy.

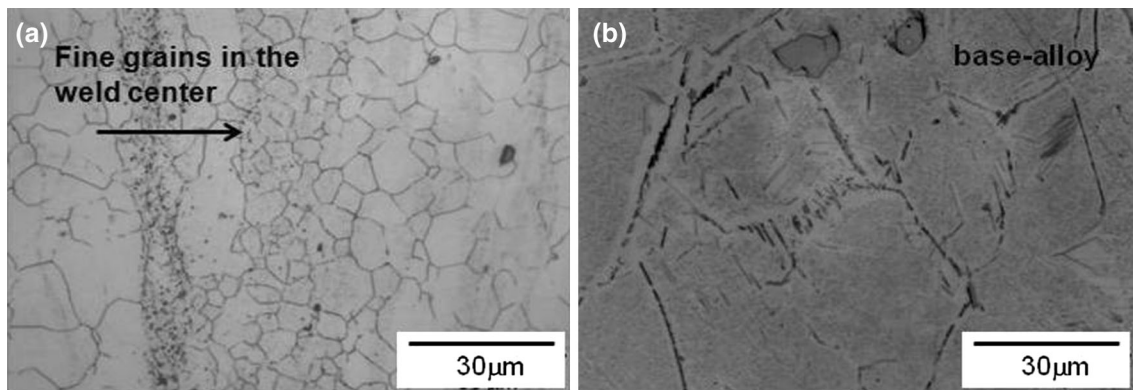


Fig. 7. (a) Recrystallized grains at the weld center and (b) grains in the base alloy; both figures have the same magnification.

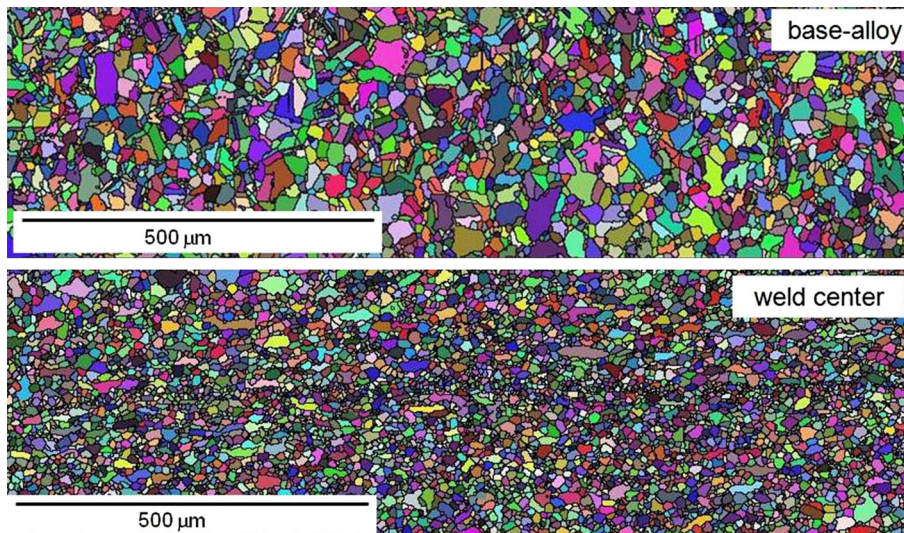


Fig. 8. EBSD-based orientation maps in the as-welded condition showing recrystallized grains in the weld center.

such phase. As can be seen from the data presented, these particles have a chemical composition that is distinctively different from those of carbides and carbonitride particles. However, the chemistry of

these particles is similar to that of δ phase and Laves phase, both of which have a similar chemical composition but very different morphologies. It was observed that the morphology of these particles is

different from that of the δ phase particles but is similar to that of Laves phase particles.² Therefore, based on the chemical analysis and morphology, these products are suggested to be Laves phase. Figure 11 shows one such particle and the corre-

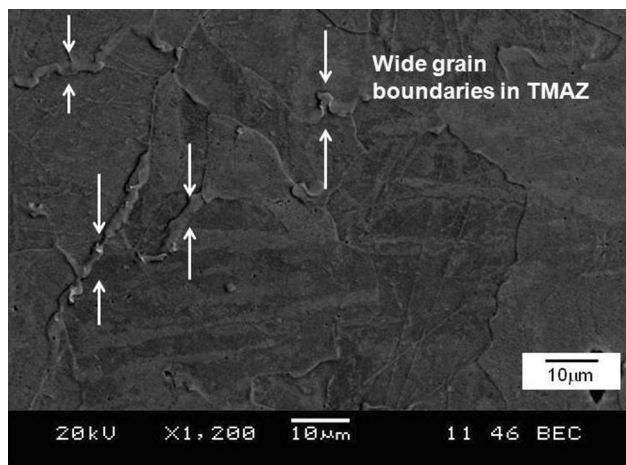


Fig. 9. Transgranular and grain boundary regions in TMAZ of as-welded 718 Plus linear friction weld.

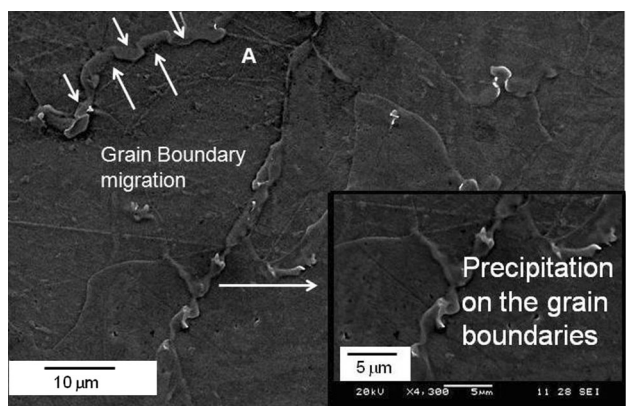


Fig. 10. LFM and precipitates on the grain boundaries in the as-welded TMAZ microstructure.

sponding EDS analysis spectrum. Laves phase particles usually form in Inconel 718 type alloys during solidification. In a previous metallurgical analysis of 718 Plus alloys, Laves phase particles were not observed in wrought alloys²; however, they can form by a solidification reaction during conventional arc welding. Hence, based on this discussion, it is suggested that Laves phase particles in linear friction-welded 718 Plus could have been produced by liquation and solidification in the form of Laves + γ eutectic. The solidification process in Inconel 718 and 718 Plus alloys is generally believed to terminate by the formation γ + Laves eutectic.^{23,24} The γ phase in the Laves + γ eutectic appears to have blended with the primary γ matrix, although a halo indicative of the resolidified γ can be observed around the Laves phase separating it from the prior γ matrix, as seen in the Fig. 11. The formation of Laves phase particles has been found to be detrimental to the mechanical properties of the alloy due to their brittle nature.²⁵ However, it is to be noted that Laves phase particles form in the weld zone in conventionally welded wrought Inconel 718, whereas Laves phase particles were not observed in the weld zone (weld center) in the linear friction-welded 718 Plus alloy. This could be attributed to strain-induced rapid solidification that prevents the formation of eutectic products within the weld zone.¹⁸

The morphology of the carbides and carbonitride particles present in the TMAZ (Fig. 12) appeared to be different from those present in the base alloy (inset in Fig. 5). The particles in the base alloy exhibited a well-defined boundary, whereas those in the TMAZ had serrated boundaries, which is typical of liquated particles. The backscattered SEM images of Ti-rich carbonitride particles and Nb-rich MC type carbides, with their EDS spectra, are shown in Figs. 12 and 13, respectively. Constitutional liquation of carbides and carbonitrides is a well-established phenomenon in conventional fusion welding of 718 type superalloys. Similar features associated with grain boundary liquation cracking in the HAZ

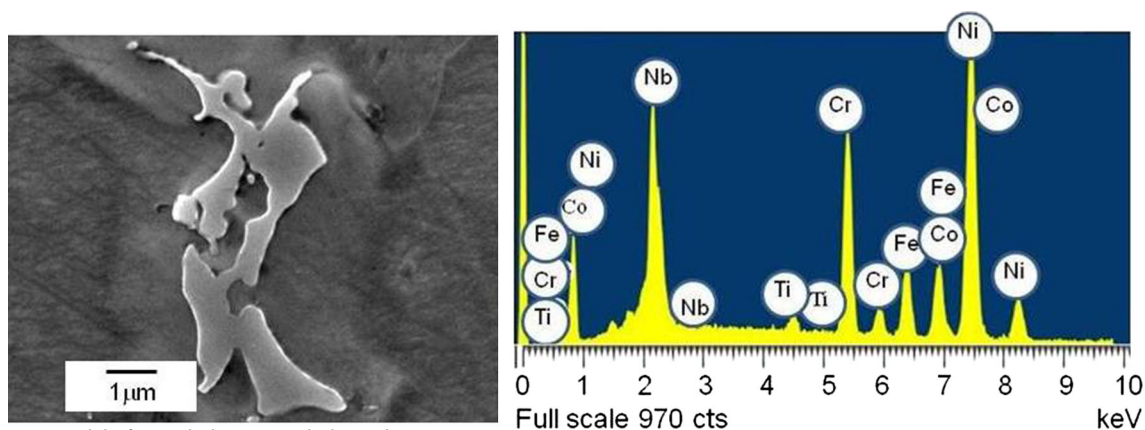


Fig. 11. Laves particle formed along a grain boundary.

of EB-welded 718 Plus were observed in a previous investigation by the current authors.^{2,26} The characteristics of the particles that appear to have formed by liquation and resolidification reactions in linear friction-welded 718 Plus are comparable with those observed in the EB welds of the alloy,²⁶ although unlike the EB welds, no microfissuring was observed during LFW. The occurrence of grain boundary liquation is not a sufficient condition for cracking to occur. Generation of sufficient tensile stresses at a time when the grain boundary regions are weakened by the presence of liquid phase is necessary to cause cracking by decohesion along one of the solid-liquid interfaces. Preclusion of intergranular cracking in the current work could be related to the imposition of compressive stress during the forging stage of the LFW process, which may have countered the driving force for cracking, that is, the tensile stress.

The δ phase particles, which are characteristically present at the base alloy grain boundaries prior to welding, were completely dissolved in the TMAZ. The rapid dissolution of δ phase particles is likely to be due to the intergranular liquation reaction involving the δ phase. The contribution of δ phase to

intergranular liquation has been reported in earlier studies in both Inconel 718 and 718 Plus alloy.^{27,28} It was proposed that δ phase particles dissociate above their solvus (about 1010°C in Inconel 718)²⁹ and enrich the grain boundary with Nb, a melting point depressant, which lowers the melting point of the grain boundary region, resulting in intergranular liquation. This is called δ phase assisted liquation.²⁸ However, Zhang and Ojo³⁰ observed that δ phase can actually constitutionally liquate in the HAZ during welding.

Postweld Heat-Treated Microstructures

PWHT is generally aimed at homogenizing the weld microstructure and relieving the residual welding stresses. In the current work, the standard PWHT for 718 Plus alloy was used. The base alloy microstructure of postweld heat-treated alloy 718 Plus consisted of coarse NbC and δ phase particles at the grain boundaries with uniform distribution of γ' precipitates within the grains, as shown in Fig. 14. A transition from the base alloy to the TMAZ is apparent in the postweld heat-treated samples by a change in the amount and distribution

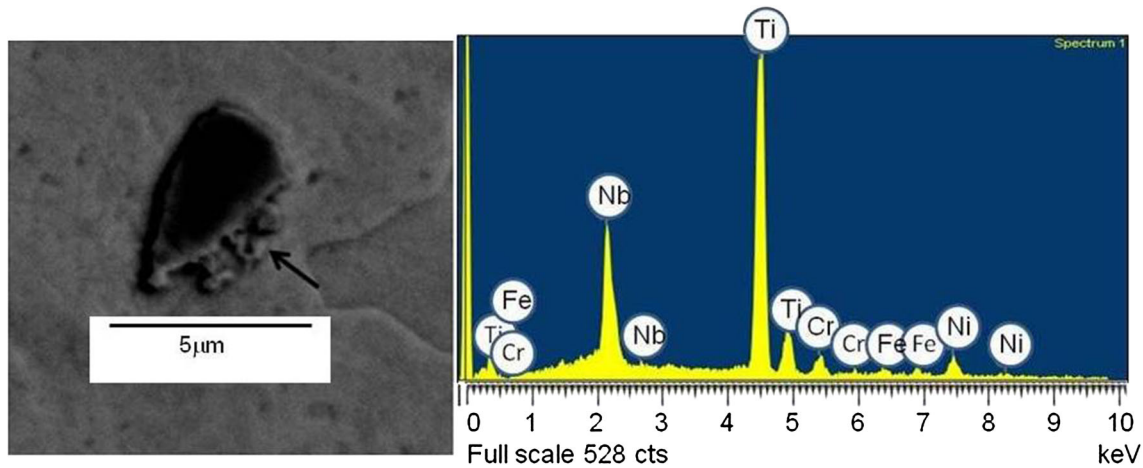


Fig. 12. Ti(C,N) particle in the TMAZ and its EDS spectrum.

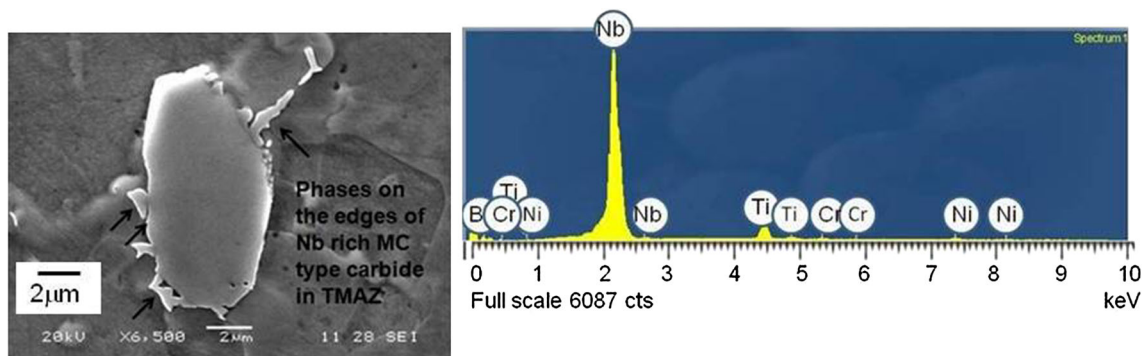


Fig. 13. MC-type carbide in the TMAZ and the associated EDS spectrum.

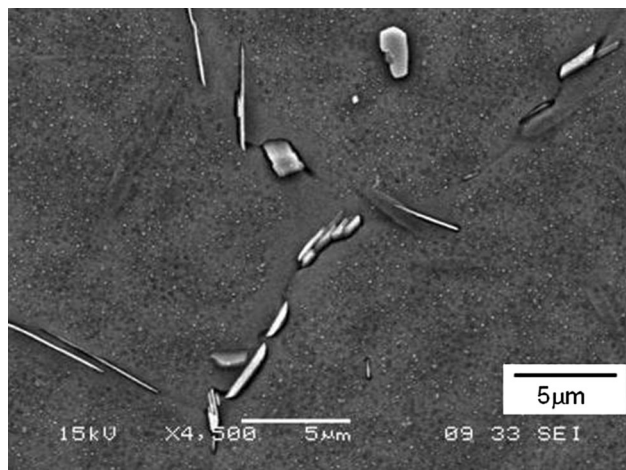


Fig. 14. Base alloy microstructure after PWHT.

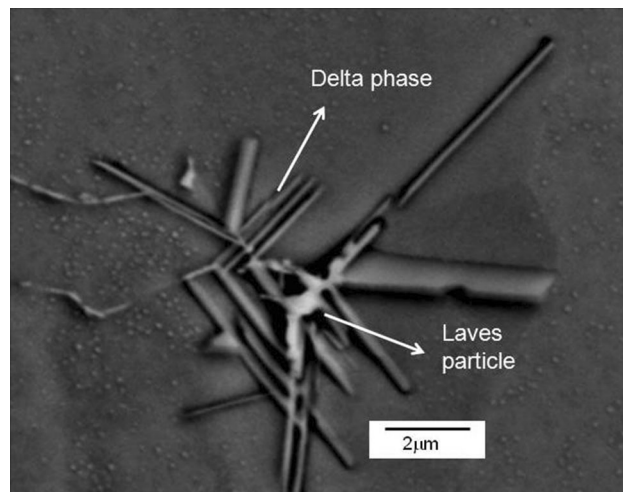


Fig. 17. Laves particle and δ phase particle in the TMAZ after PWHT.

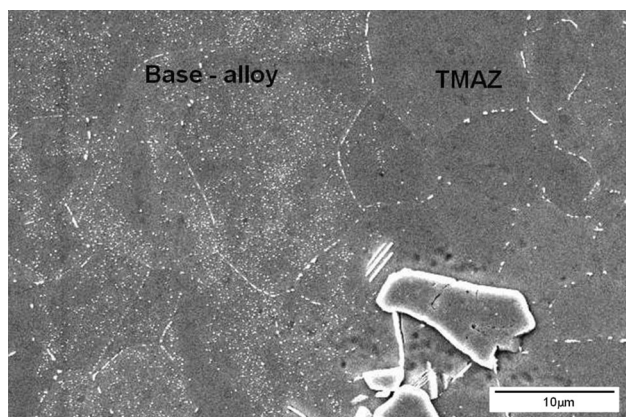


Fig. 15. Transition from base alloy to TMAZ microstructure in post-weld heat-treated alloy.

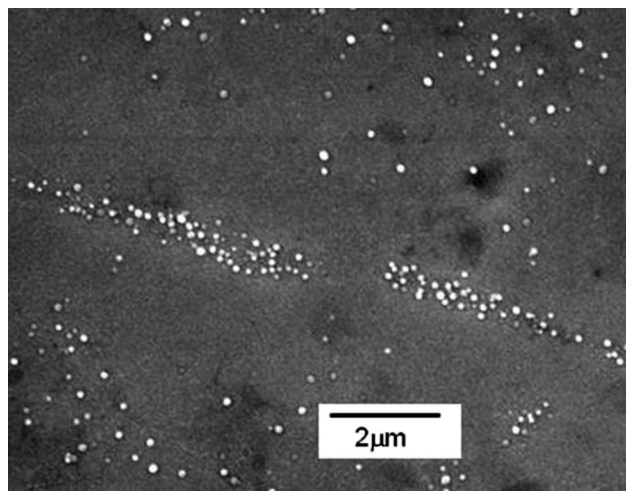


Fig. 16. Nonuniform distribution of γ' phase in the TMAZ of postweld heat-treated 718 Plus weld.

of second-phase particles. A marked difference in the amount of γ' particles was observed between the TMAZ and base alloy. It was observed that the extent of γ' precipitation in TMAZ was considerably less than that observed in the base alloy, and the distribution seems to be nonuniform in nature (Fig. 15). Similarly, the extent of δ phase precipitation was less in the TMAZ compared to that in the base alloy, and the particles were more pronounced in certain regions within the grains and around certain phases. Figure 16 shows a grain boundary in the TMAZ region of the postweld heat-treated weld that exhibited clusters of precipitates. One significant observation is that the intergranular and transgranular regions that appear to have liquated during welding, consistently showed a higher extent of δ phase precipitation.

PWHT could not eliminate the Laves particles that formed during the welding process, rather δ phase precipitation was observed around them, as shown by one such case in Fig. 17. Similarly, increased precipitation of δ phase was observed around carbides and carbonitride particles (Figs. 17 and 18). A comparison of Figs. 18 and 14 shows that, unlike in the TMAZ region, carbide and carbonitrides particles in the base alloy in the postweld heat-treated condition do not have any Laves particles associated with them. Because Laves phase can only form during solidification from the liquid state, this observation further supports the suggestion that liquation likely occurred in the TMAZ during LFW.

Similar to the as-welded condition, no microfissuring was observed in the postweld heat-treated linear friction-welded 718 Plus alloy. The current work indicates that with the process parameters used, 718 Plus can be welded by the LFW process without cracking. However, phase reactions that

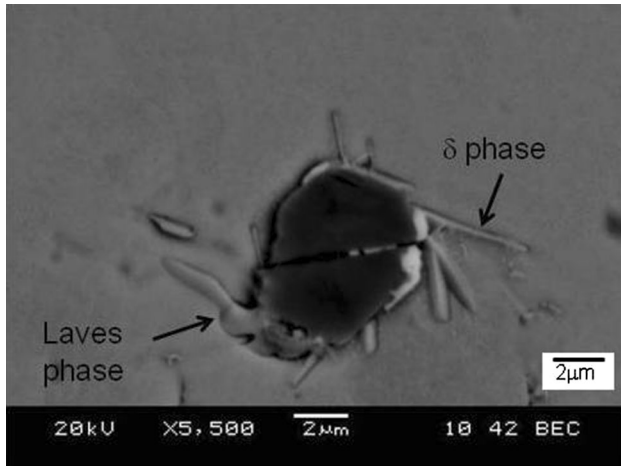


Fig. 18. Ti-carbonitride particles with δ phase and Laves phase in the postweld heat-treated condition.

occurred during welding appear to result in the formation of Laves phase particles, which are known to be detrimental to the mechanical properties. Also, non-uniform distribution of precipitates after the PWHT, including that of the γ' phase, could adversely affect the high-temperature properties of the alloy. Hence, the occurrence of liquation and its likely influence on postweld heat-treated microstructure are important factors that merit more in-depth consideration for qualifying the application of LFW to 718-type alloys.

SUMMARY AND CONCLUSION

1. LFW of Inconel 718 Plus with a frequency of 100 Hz, pressure of 90 MPa, amplitude of 2 mm, and axial shortening of 2 mm produced a sound weld without microfissuring.
2. The weld region consisted of fine recrystallized grains, and although intergranular liquation appears to have occurred in the TMAZ, weld cracking was not observed.
3. Grain boundary liquation resulted in the formation of Laves phase and inhomogeneous precipitation of the principle-strengthening precipitate γ' during PWHT.
4. The absence of microfissuring in the linear friction-welded alloy may be attributed to the compressive stresses applied to the joint region during the forging phase of LFW, which may be responsible for the absence of resolidification eutectic products in the weld center.

ACKNOWLEDGEMENTS

The authors would like to thank Natural Sciences and Engineering Research Council of Canada for

the financial support. The technical assistance of M. Guerin and E. Dalgaard for LFW of IN 718 Plus is also greatly appreciated.

REFERENCES

1. W.D. Cao and R. Kennedy, *Superalloys*, ed. K.A. Green, T.M. Pollock, H. Harada, T.E. Howson, R.C. Reed, J.J. Schirra, and S. Walston (Warrendale, PA: TMS, 2004), pp. 91–99.
2. K.R. Vishwakarma, N.L. Richards, and M.C. Chaturvedi, *Mater. Sci. Eng. A Struct.* 480, 517 (2008).
3. O. Idowu, O.A. Ojo, and M.C. Chaturvedi, *Mater. Sci. Eng. A Struct.* 454–455, 389 (2006).
4. A. Varis and M. Frost, *Mater. Sci. Eng. A Struct.* 292, 8 (2000).
5. I. Bhamji, M. Preuss, P.L. Threadgill, R.J. Moat, A.C. Addison, and M.J. Peel, *Mater. Sci. Eng. A Struct.* 528, 680 (2010).
6. E. Dalgaard, P. Wanjara, J. Gholipour, and J.J. Jonas, *Can. Metall. Q.* 51, 269 (2012).
7. E. Dalgaard, P. Wanjara, J. Gholipour, X. Cao, and J.J. Jonas, *Acta Mater.* 60, 770 (2012).
8. A. Chamanfar, M. Jahazi, J. Gholipour, P. Wanjara, and S. Yue, *Mater. Sci. Eng. A Struct.* 555, 117 (2012).
9. O.T. Ola, O.A. Ojo, P. Wanjara, and M.C. Chaturvedi, *Adv. Mater. Res.* 278, 446 (2011).
10. S.V. Lalam, G.M. Reddy, T. Mohandas, M. Kamaraj, and B.S. Murty, *Mater. Sci. Tech. Ser.* 25, 851 (2009).
11. P. Wanjara, E. Dalgaard, J. Gholipour, and J. Larose, *Mater. Sci. Forum* 706–709, 3022 (2012).
12. A. Chamanfar, M. Jahazi, J. Gholipour, P. Wanjara, and S. Yue, *Mater. Des.* 36, 113 (2012).
13. O.T. Ola, O.A. Ojo, P. Wanjara, and M.C. Chaturvedi, *Metall. Mater. Trans. A* 43A, 921 (2012).
14. O.T. Ola, O.A. Ojo, P. Wanjara, and M.C. Chaturvedi, *Metall. Mater. Trans. A* 42A, 3761 (2011).
15. P. Wanjara and M. Jahazi, *Metall. Mater. Trans. A* 36A, 2149 (2005).
16. C. Mary and M. Jahazi, *Adv. Mater. Res.* 15–17, 357 (2007).
17. A. Chamanfar, M. Jahazi, J. Gholipour, P. Wanjara, and S. Yue, *Metall. Mater. Trans. A* 44, 4230 (2013).
18. O.T. Ola, O.A. Ojo, P. Wanjara, and M.C. Chaturvedi, *Philos. Mag. Lett.* 91, 140 (2011).
19. A. Chamanfar, M. Jahazi, J. Gholipour, P. Wanjara, and S. Yue, *Metall. Mater. Trans. A* 42, 729 (2011).
20. J.J. Pepe and W.F. Savage, *Weld J.* 9, 411-s (1967).
21. R. Nakkalil, N.L. Richards, and M.C. Chaturvedi, *Acta Metall. Mater.* 41, 3381 (1993).
22. O.A. Ojo, N.L. Richards, and M.C. Chaturvedi, *Scr. Mater.* 51, 141 (2004).
23. B. Radhakrishnan and R.G. Thompson, *Metall. Trans. A* 20A, 2866 (1989).
24. B. Radhakrishnan and R.G. Thompson, *Metall. Trans. A* 23A, 1783 (1992).
25. J.J. Schirra, R.H. Caless, and R.W. Hatala, *Superalloys 718, 625, 706 and Various Derivatives*, ed. E.A. Loria (Warrendale, PA: TMS, 1991), pp. 375–388.
26. K.R. Vishwakarma, N.L. Richards, and M.C. Chaturvedi, *Superalloys 718, 625, 706 and Various Derivatives*, ed. E.A. Loria (Warrendale, PA: TMS, 2006), pp. 637–647.
27. Q. Li (Ph.D. thesis, University of Manitoba, 2006).
28. M. Qian and J.C. Lippold, *Acta Mater.* 51, 3351 (2003).
29. S. Azadian, L. Wei, and R. Warren, *Mater. Charact.* 57, 7 (2004).
30. H.R. Zhang and O.A. Ojo, *Philos. Mag. Lett.* 89, 787 (2009).